

The Frequency Selection of SH0 Waves for Total Transmission and Its Application in the Damage Detection of Aircrafts

Yanchao Yue^{1,*}, Tangbing Chen¹, Lingling Zhang¹, Moustafa Abdelsalam¹ and Josephine Musanyufu¹

Abstract: Based on wave interference, a methodology to realize the total transmission phenomenon of SH0 waves is proposed in this paper. After a systematical theoretical investigation, an exact frequency of a flat plate consisting of another medium with finite length, is obtained, which is furthermore exemplified by the finite element method. This frequency is the same as the classical Fabry-Perot condition and dependent on the thickness of the material. It has been revealed that an SH0 wave, with its wavelength equal to twice of the length of another medium, can totally transmit across the medium without reflection. Especially when the impedance changes in a specific range, the energy of transmitted waves can keep in a high level, which is frequency-independent. Not limited by a flat plate, the Fabry-Perot condition is also suitable for a scraggy plate when the thickness variation is relatively small. Finally, using the transfer matrix method, the wave propagation in a plate with multiple layers is quantitatively investigated, and the frequency analysis for total transmission is carried out. The methodology, as well as the design scheme proposed, is achievable and artificially controllable, which opens a new prospect for the wave control and final applications in aeronautics and astronautics.

Keywords: Shear horizontal waves, total transmission, Fabry-Perot condition, impedance.

1 Introduction

Structural health monitoring (SHM) and non-destructive evaluation (NDE) techniques are usually used to detect structural damages in aircrafts. As a general technique extensively applied in SHM and NDE systems, ultrasonic guided wave inspection, has been proven its effectiveness and tremendous value for detecting the damage [Mitra and Gopalakrishnan (2016); Dai, Jing, Sun et al. (2018)]. Two kinds of traditional guided waves are usually used in a thin plate-type structure, i.e., Lamb waves and shear horizontal (SH) waves. Owing to some special characteristics, such as high sensitivity to damage, easy generation and reception, omnidirectional dissemination, long-distance transmission, and so forth, the Lamb wave-based techniques have been successfully applied in SHM systems [Mitra and Gopalakrishnan (2016); Dai, Jing, Sun et al. (2018); Stepinski, Mańka and Martowicz (2017); Dai, Jing, Wang et al. (2018)]. However, Lamb

¹ Department of Civil Engineering, Xi'an Jiaotong University, Xi'an, 710049, China.

* Corresponding Author: Yanchao Yue. Email: yuey@xjtu.edu.cn.

Received: 09 May 2019; Accepted: 11 June 2019.

wave is dispersive. In other words, its phase velocity and group velocity are related to the excitation frequency and the plate thickness, which inevitably increases complexity for the signal processing. Especially, in order to satisfy the velocity matching conditions, the dispersion property seriously limits the frequency selection when the second-harmonic Lamb wave is used for the early detection of micro-damages [Pruell, Kim, Qu et al. (2009)]. By contrast, the lowest order mode of SH waves, or the fundamental shear horizontal (SH0) wave, exhibits its unique superiority because it is non-dispersive, i.e., its phase and group velocities are only determined by material parameters, not related to the external frequency. Because of the frequency-independent characteristics, the incident wave will keep its original profile without distortion, which can efficiently simplify the interpretation and identification of received signals [Kamal and Giurgiutiu (2014); Zhou, Li and Yuan (2015)]. Additionally, the frequency can be chosen at random when the third-harmonic SH wave is used for detecting the early stage of micro-damages, not limited by the velocity matching conditions [Lissenden, Liu, Choi et al. (2014)]. Meanwhile, no mode conversion happens when SH0 waves encounter defects or boundaries, which is beneficial for signal processing [Belanger and Boivin (2016)]. Hence, the SH0 wave-based techniques are expected to be explored and developed for SHM. Additionally, SH waves are also used in other regions, such as Surface Acoustic Wave (SAW) devices [Cao, Jin, Jeon et al. (2009)], ultrasonic imaging technology [Sarvazyan, Rudenko, Swanson, et al. (1998)], and so forth. As the priority of engineering application, the transmission property is always crucial and becomes an important issue concerned.

The first step of successfully applying SH0 wave-based techniques into SHM system is the wave generation. In order to generate a relative pure SH0 signal, several attempts are developed, such as interdigital PVDF [Wilcox, Cawley and Lowe (1998); Wang, Quek and Varadan (2005)], electromagnetic acoustic transducer (EMAT) [Lee, Kim and Cho (2009)], shear horizontal piezoelectric wafer active sensor (SH-PWAS) [Kamal and Giurgiutiu (2014); Zhou, Li and Yuan (2015); Miao, Dong and Li (2016); Li, Shan, Wen et al. (2019)], and so forth. During the wave excitation, how to choose a frequency appropriately is the priority. On the one hand, the wave amplitude of SH0 wave is required as large as possible, and meanwhile without the interference of Lamb waves [Kamal and Giurgiutiu (2014); Miao, Dong and Li (2016)]. On the other hand, the generated waves should keep a high transmission level when they encounter another media through a proper excitation frequency beforehand, which is the origin, as well as the novelty, of the present contribution.

In this paper, a systematic theoretical investigation is carried out and an exact frequency expression is proposed for the total transmission of SH0 waves in a flat plate embedded in another medium with finite length. After validation via finite element method (FEM), its application in SHM has been demonstrated in detail in Section 2. In the following, the frequency selection in a scraggy plate is qualitatively analyzed in Section 3, and then quantitatively illustrated in Section 4 when SH0 wave propagates in a multilayered plate. Finally, some remarks are concluded in Section 5. This work can lay the groundwork for the theory extension, explanation of certain physical phenomenon, structural optimization, experimental measurement evidence, and final engineering applications.

2 The total transmission of SH0 waves in a flat plate

Aircrafts are usually made of composite materials, which inevitably induce the impedance mismatch at the joint of different components. When using wave-based technique to detect damages, wave reflections will appear evidently and further seriously affect the final detection accuracy. In order to solve the total transmission of SH0 wave when it encounters another medium, a sandwich structure shown in Fig. 1 is considered. An infinite thin plate is composed of two different media with the shear modulus μ_1 and μ_2 and mass density ρ_1 and ρ_2 . The plate thickness is denoted by h and L represents the length of the midsection. It is assumed that an incident SH0 wave from $-\infty$ travels along the positive direction of x -axis, and go through Medium 2. Mostly, the first reflected wave and transmitted wave are used for detecting cracks and defects in the matrix, i.e., distributed in the region of $x > L$. However, the second reflected wave can be adopted to detect defects inside the Medium 2. Additionally, by comparison the first and transmitted wave signals, the material properties of Medium 2 (Elastic modulus, Poisson’s ratio and mass density) can be derived. Therefore, investigation the wave reflection and transmission in composite structures is significant. Our aim is to choose the excitation frequency, so that the incident SH0 wave can totally transmit the midsection and propagate further without reflection.

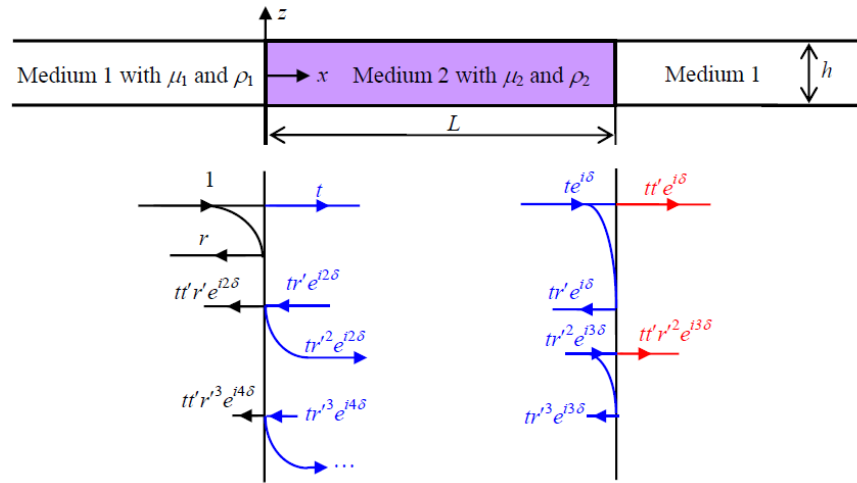


Figure 1: The theoretical model and the wave propagation process

2.1 Theoretical analysis

In an elastic plate, the displacement components of pure SH waves can be represented by [Li, Shan, Wen et al. (2019); Danoyan and Piliposian (2008); Golub, Fomenko, Bui et al. (2012); Li and Cheng (2018)]

$$u_x = u_z = 0, u_y = u(x, z, t) \tag{1}$$

which obey the following two-dimensional dynamic governing equation [Li, Shan, Wen et al. (2019); Danoyan and Piliposian (2008); Golub, Fomenko, Bui et al. (2012); Li and Cheng (2018); Qian, Liu, Yang et al. (2010)].

$$\mu \left(\frac{\partial^2 u_y}{\partial x^2} + \frac{\partial^2 u_y}{\partial z^2} \right) = \rho \frac{\partial^2 u_y}{\partial t^2} \quad (2)$$

here ρ and μ are respectively the mass density and shear modulus of the plate, and then the corresponding phase velocity of non-dispersive SH0 waves can be calculated as $c_{\text{SH0}} = \sqrt{\mu / \rho}$.

The reflection and transmission processes in the time domain are depicted in Fig. 1. It should be stressed here in order to distinguish the different wave components during reflection and transmission processes, Fig. 1 has separated them along the plate thickness. According to Eqs. (1) and (2), the shear displacement of incident waves with unit amplitude can be expressed as $u_{\text{in}} = \exp[i(k_1 x - \omega t)]$, in which the wave number is $k_1 = \omega / c_1$. $\omega = 2\pi f$ denotes the angular frequency, and the phase velocity are determined by $c_1 = \sqrt{\mu_1 / \rho_1}$. It is assumed that the reflected and transmitted coefficients of u_y are respectively r and t when the wave encounters Medium 2 from Medium 1, and r' and t' vice versa. Therefore, when the incident SH0 wave firstly arrives at the interface $x=0$, the reflected and transmitted waves can be respectively written as $r \exp[i(k_1 x + \omega t)]$ and $t \exp[i(k_2 x - \omega t)]$ with $k_2 = \omega / c_2$ and $c_2 = \sqrt{\mu_2 / \rho_2}$, such as Fig. 1. When it gets at $x=L$, it becomes $t e^{i\delta} \exp[i(k_2 x - \omega t)]$ with $i\delta = ik_2 L$ denoting the phase difference of the transmitted SH0 wave between $x=0$ and $x=L$. Furthermore, the amplitudes of waves launching from $x=L$ are respectively $tt' e^{i\delta} \exp[ik_1(x-L) - i\omega t]$ for right-traveling transmitted wave and $tr' e^{i\delta} \exp[i(k_2 x + \omega t)]$ for left-traveling reflected wave. For the left-traveling wave, the same reflection and transmission phenomena will take place continuously. Finally, the reflected wave can be expressed as the summation of all n th reflected waves in the region of $x > 0$, i.e.,

$$\begin{aligned} u^R &= r \exp[i(k_1 x + \omega t)] + tt' r' e^{i2\delta} \exp[i(k_1 x + \omega t)] + tt' r'^3 e^{i4\delta} \exp[i(k_1 x + \omega t)] + \dots \\ &= \left[r + tt' r' e^{i2\delta} (1 + r'^2 e^{i2\delta} + \dots) \right] \exp[i(k_1 x + \omega t)] \\ &= \left(r + tt' r' e^{i2\delta} \frac{1}{1 - r'^2 e^{i2\delta}} \right) \exp[i(k_1 x + \omega t)] \end{aligned} \quad (3)$$

It is common that the n th reflected wave will become smaller and smaller; and thus has been viewed as zero in Eq. (3). In order to obtain the reflected and transmitted coefficients r , t , r' , and t' , boundary conditions corresponding for displacement and stress components at $x=0$ and $x=L$ in the frequency domain will be considered. Taking $x=0$ for example, the continuity of stress and displacement requires [Li, Shan, Wen et al. (2019); Li and Cheng (2018)].

$$\begin{cases} 1+r=t, \\ \mu_1 k_1 (1-r) = \mu_2 k_2 t, \end{cases} \quad (4)$$

From which we can get

$$r = \frac{n_{21}-1}{1+n_{21}}, \quad t = \frac{2n_{21}}{1+n_{21}}, \quad (5)$$

With the impedance $n_{21} = \frac{\rho_1 \mu_1}{\rho_2 \mu_2}$. Similarly, at $x=L$, using the similar equations, r' and t' can

be obtained as

$$r' = \frac{1-n_{21}}{1+n_{21}} = -r, \quad t' = \frac{2}{1+n_{21}}. \quad (6)$$

Submitting Eqs. (5) and (6) into Eq. (3) yields

$$\begin{aligned} u^R &= \left[r - r(1-r^2)e^{i2\delta} \frac{1}{1-r^2e^{i2\delta}} \right] \exp[i(k_1x + \omega t)] \\ &= r \left[1 - (1-r^2)e^{i2\delta} \frac{1}{1-r^2e^{i2\delta}} \right] \exp[i(k_1x + \omega t)] \\ &= r \frac{1-e^{i2\delta}}{1-r^2e^{i2\delta}} \exp[i(k_1x + \omega t)]. \end{aligned} \quad (7)$$

Therefore, the energy of the reflected wave can be expressed as

$$\begin{aligned} I^R &= u^R \bar{u}^R = r^2 \frac{1-e^{i2\delta}}{1-r^2e^{i2\delta}} \frac{1-e^{-i2\delta}}{1-r^2e^{-i2\delta}} = r^2 \frac{2-2\cos(2\delta)}{1-2r^2\cos(2\delta)+r^4} \\ &= r^2 \frac{4\sin^2\delta}{(1-r^2)^2 + 4r^2\sin^2\delta} = \frac{F\sin^2\delta}{1+F\sin^2\delta}. \end{aligned} \quad (8)$$

Here the overbar is used to denote complex conjugate, and $F = \frac{4r^2}{(1-r^2)^2}$. Using the same

method, the transmitted SH0 wave can be obtained as

$$\begin{aligned} u^T &= tt'e^{i\delta} (1+r'^2e^{i2\delta} + \dots) \exp[ik_1(x-L) - i\omega t] \\ &= tt'e^{i\delta} \frac{1}{1-r'^2e^{i2\delta}} \exp[ik_1(x-L) - i\omega t]. \end{aligned} \quad (9)$$

Furthermore, its energy is

$$I^T = u^T \bar{u}^T = (1-r^2)^2 \frac{e^{i\delta}}{1-r^2e^{i2\delta}} \frac{e^{-i\delta}}{1-r^2e^{-i2\delta}} = \frac{(1-r^2)^2}{1-2r^2\cos(2\delta)+r^4} = \frac{1}{1+F\sin^2\delta}. \quad (10)$$

From Eqs. (8) and (10), we can obtained that $I^R + I^T = 1$, i.e., the principle of energy conservation, which can efficiently validate the theoretical process to some extent. Especially, in order to make sure the incident SH0 wave totally transmitted, i.e., $I^T = 1$ or $I^R = 0$, we can achieve $\sin\delta = 0$. In this case, $k_2L = m\pi$ with $m = 1, 2, 3, \dots$. It is anticipated that a pure SH0 wave can be generated without other higher SH wave

components, and thus the lowest excitation frequency can be obtained when $m=1$, i.e.,

$$f_0 = \frac{c_2}{2L}. \quad (11)$$

In other words, $\lambda=2L$, i.e., the wavelength of inherent SH0 wave propagation in the middle medium equals to $2L$. Eq. (11) is the same as the classical Fabry-Perot condition and dependent on the thickness of the material. Until to now, it has been revealed theoretically that the SH0 wave with its frequency shown in Eq. (11) can totally transmit without reflection when it encounters another medium.

2.2 Numerical validations

In the previous section, the frequency of SH0 waves, corresponding for total transmission when the wave encounters another finite medium that is different from the matrix material, has been derived theoretically. In this section, this phenomenon will be validated numerically and furthermore applied in SH0 wave-based SHM systems.

In order to prove the correctness of Eq. (11), an aluminum plate, with its mass density $\rho_1=2730 \text{ kg/m}^3$ and shear modulus $\mu_1=28.5 \text{ GPa}$ is adopted as the numerical simulation [Pennec, Djafari-Rouhani, Larabi et al. (2008)]. Meanwhile, it is assumed that the region of $0 \leq x \leq L$ is respectively occupied by two different kinds of materials, i.e., epoxy ($\rho_2=1142 \text{ kg/m}^3$ and $\mu_2=1.48 \text{ GPa}$) with $n_{21}=6.78>1$ and silicon ($\rho_2=2331 \text{ kg/m}^3$ and $\mu_2=79.62 \text{ GPa}$) with $n_{21}=0.65<1$ [Pennec, Djafari-Rouhani, Larabi et al. (2008)]. Using these data, the variation of energy for reflected and transmitted waves with the frequency can be calculated, such as the black and red solid lines in Fig. 2. On the other hand, a FEM model, i.e., an aluminum flat plate with its thickness 5 mm, is established in the frequency domain in COMSOL software, such as Fig. 3. An SH0 wave propagation along the $+x$ direction is generated at the region $-3 \text{ cm} \leq x \leq 0$ via the artificial setting of background field and detected at $x=1.5 \text{ cm}$. Medium 2 is chosen as the epoxy or silicon. Meanwhile, two perfect matched layers (PMLs) are added as the extended regions that can mimic the infinity boundaries. Quadrilateral elements are adopted to discretize the structure. For the wave transmission calculation, the element size is typically chosen as 0.1 mm, i.e., one twentieth of the wavelength. After changing the excitation frequencies, I^R and I^T can be calculated and shown by the rectangular and star symbols in Fig. 2.

The theoretical results are coincident as that from FEM in Fig. 2, which can effectively prove the correctness of our theoretical calculations. On the other hand, $I^T=1$ and $I^R=0$ at $f=c_2/2L$ for both $n_{21}>1$ and $n_{21}<1$ cases, which is consistent with the prediction of Eq. (11). The variations of I^T and I^R are periodic, which is caused by the trigonometric functions in Eqs. (8) and (10). Therefore, multiple frequencies, corresponding for total transmission of SH0 waves, appears and can be expressed as $f=mc_2/2L$, which is also the same as the theoretical prediction above. It should be noted here that $I^R + I^T = 1$ always keep in Fig. 2, which dues to the principle of energy conservation [Xu (2015); Li and Cheng (2017)].

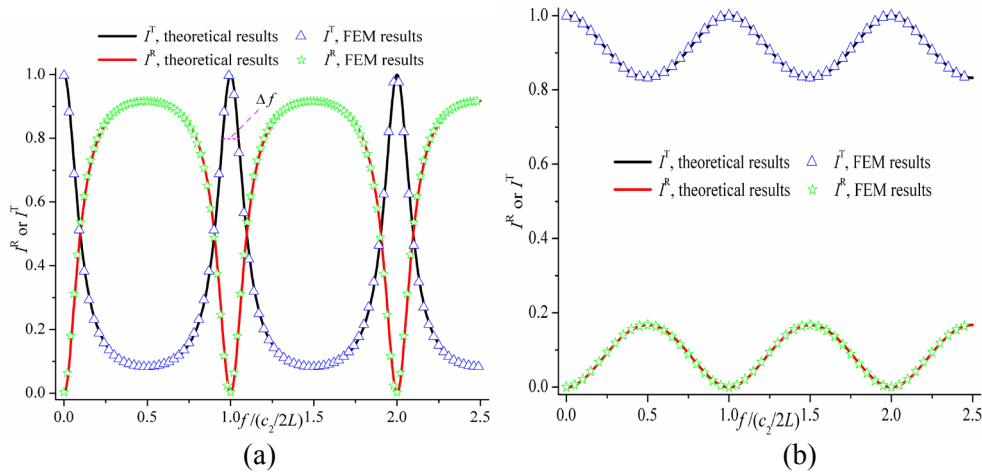


Figure 2: The comparison between theoretical and FEM results when Medium 2 is chosen as (a) epoxy and (b) silicon

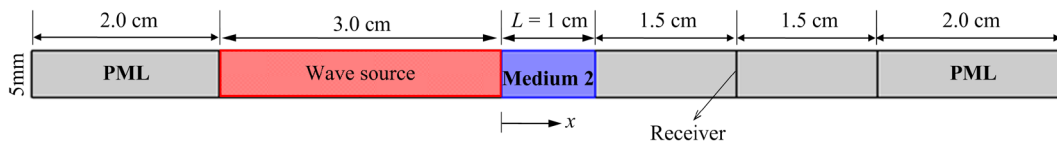


Figure 3: The model established in the COMSOL software

Except for the transmission spectrum in Fig. 2, the displacement fields of incident and transmitted waves output from COMSOL at $f=c_2/2L$ are shown in Fig. 4. For cases of epoxy and silicon, the incident SH0 wave hardly reflects and transmits totally when it encounters to Medium 2, which proves the correctness of our theoretical prediction again.

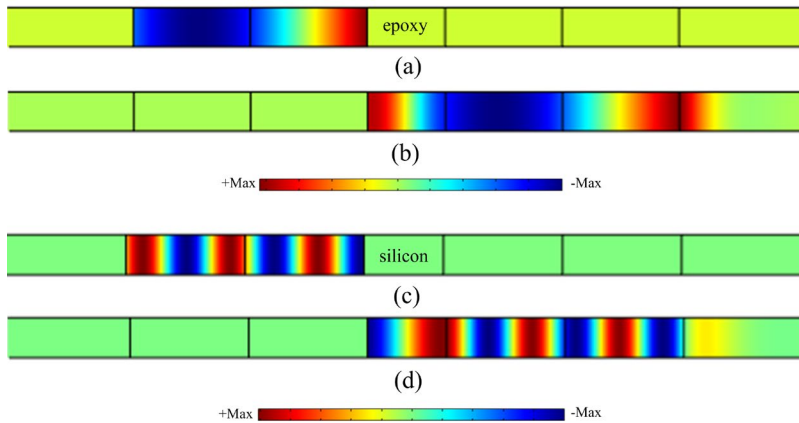


Figure 4: The displacement fields of SH0 waves for different conditions: (a) is u_{in} ; (b) represents u^R and u^T if Medium 2 is chosen as epoxy when the excitation frequency is $f=c_2/2L=56.92$ kHz; (c) is u_{in} ; (d) represents u^R and u^T if Medium 2 is chosen as silicon when the excitation frequency is $f=c_2/2L=292.22$ kHz

2.3 Application in SHM

In SHM, tone-burst excitations are usually adopted for damage diagnoses, so that the incident SH0 wave has a bandwidth centered at a selected frequency. Therefore, it is important to choose a proper frequency bandwidth centered at $f=c_2/2L$. For example, if let 80% of incident energy can transmit at $x=L$, such as Fig. 2, the frequency bandwidth Δf can be obtained. In this case, $F \sin^2 \delta=1/4$ can be derived from Eq. (10), and then a non-dimensional frequency bandwidth $\Delta f/f_0$ can be calculated as

$$\frac{\Delta f}{f_0} = \frac{2}{\pi} \arcsin\left(\frac{1-r^2}{4r}\right), \quad (12)$$

With its variation versus the changing of n_{21} shown in Fig. 5, which can provide us the structural optimal scheme. The central frequency f_0 can be calculated firstly with the aid of Eq. (11), and then the bandwidth of input tone-burst signal can be determined according to Fig. 5. It should be stressed here that the non-dimensional frequency bandwidth $\Delta f/f_0$ always keeps unit (the blue line in Fig. 5) when $0.62 < n_{21} < 1.61$. In other words, if n_{21} locates in the region of (0.62, 1.61), the central frequency f_0 , as well as the bandwidth Δf , can be chosen randomly for generation, the energy of transmitted SH0 waves can be kept above 80%. In order to prove the correctness, Medium 2 with its $n_{21}=0.7$ is adopted, and the transmission energy I^T has been calculated via theory and FEM, such as the sub-figure in Fig. 5. The minimum of I^T is about 0.88, larger than 0.8, which can efficiently prove the correctness of the analysis.

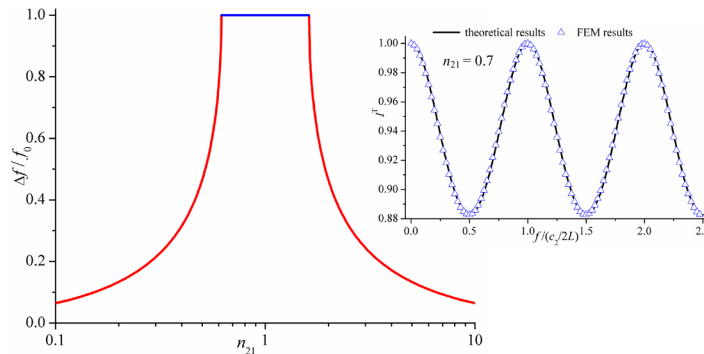


Figure 5: The variation of $\Delta f/f_0$ versus the impedance n_{21}

It should be emphasized that Eq. (12) and Fig. 5 are only suitable for the assumption that 80% of the incident SH0 wave can transmit. If other value required is concerned, another frequency bandwidth will be obtained. In present contribution, we just propose a methodology for analysis. However, this methodology is general and can be extensively applied easily.

3 The total transmission of SH0 waves in a scraggy plate

When detecting crack and micro-holes using guided waves, it is common that the incident wave encounters an abrupt section in a plate-type structure. Considering the influence of the abrupt thickness on the total transmission property, the theoretical model in Fig. 1 has

been generalized, such as Fig. 6. Medium 2 has an abrupt thickness, i.e., $h_2 \neq h_1$. Under this condition, the total transmission of SH0 waves will be discussed in this section.

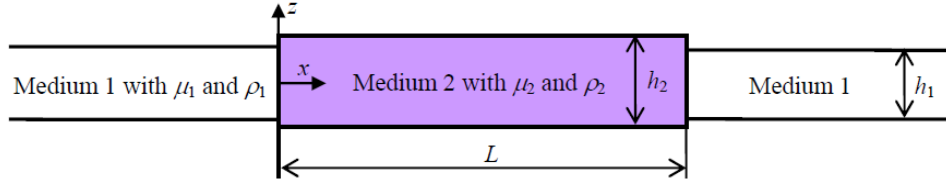


Figure 6: A scraggy plate

The theoretical analysis is the same as Fig. 2 except the reflected and transmitted coefficients in Eqs. (5) and (6), because an exact boundary conditions at the mismatched interfaces $x=0$ and L cannot be satisfied. Instead, if the thickness variation is tiny, an approximation, i.e., the displacement and the moment of shear stress are continuous across the interfaces, is assumed here [Li and Cheng (2017); Zhu, Chen and Yang (2014)], which yields

$$\begin{cases} 1+r=t, \\ h_1\mu_1k_1(1-r)=h_2\mu_2k_2t. \end{cases} \quad (13)$$

Similarly, the approximate boundary condition at $x=L$ can also be achieved. Then, the reflected coefficients (r and r'), as well as the transmitted coefficients (t and t') can be derived, with their expressions are the same as before if the impedance n_{21} is replaced by $\frac{h_1}{h_2}n_{21}$. Therefore, it is predictable that the excitation frequency of SH0 waves

corresponding for total transmission is still $f_0=c_2/2L$, which is the intrinsic property and are not affected by the plate thickness. To some extent, Fig. 6 is equivalent to Fig. 1 with the impedance $n_{21} = \frac{h_1}{h_2} \frac{\rho_1\mu_1}{\rho_2\mu_2}$.

For FEM verification, the materials adopted in Section 2.2 are used here except $h_2=0.8 h_1$, and the corresponding displacement distribution is depicted in Fig. 7. The generation frequency is chosen as $f=c_2/2L$, and the incident wave almost totally transmit without reflection. It is consistent with Fig. 4, which can prove the correctness of the theoretical prediction. Here, the assumption used in Eq. (13) is only suitable for the small thickness difference. Caused by the approximate Fabry-Perot condition, a tiny reflected wave appears in the region of $x<0$ in Fig. 7. However, this small reflection is negligible for SHM. In a word, this analytical method is proper when the ratio h_2/h_1 approaches to 1, which is easy and provides us an explicit frequency for wave generation.

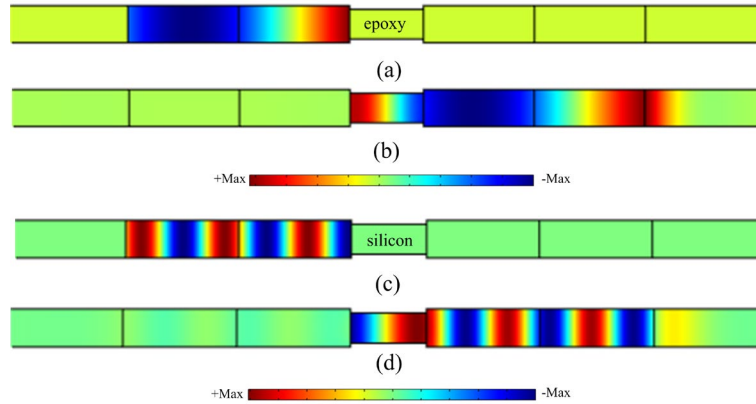


Figure 7: The displacement fields of SH0 waves in a scraggy plate when $h_2=0.8h_1$: (a) is u_{in} ; (b) represents u^R and u^T if Medium 2 is chosen as epoxy when the excitation frequency is $f=c_2/2L=56.92$ kHz; (c) is u_{in} ; (d) represents u^R and u^T if Medium 2 is chosen as silicon when the excitation frequency is $f=c_2/2L=292.22$ kHz

4 The total transmission of SH0 waves in a multilayered plate

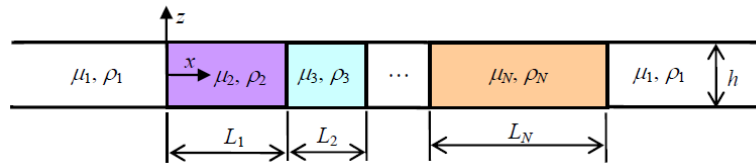


Figure 8: An inhomogeneous plate with N -layers

In order to further investigate the total transmission of SH0 waves in a multiple-layered structure, a flat plate consisting of N sections, shown in Fig. 8, is adopted in this section, and the transfer matrix method [Xu (2015); Li and Cheng (2017)] is used during the theoretical derivation process. If there is only one sub-layer, we can assume that the displacement u_y in the region $0 < x < L_1$ can be expressed as $u_y = U_1 \exp[i(k_1x - \omega t)] + U'_1 \exp[i(k_1x + \omega t)]$. The boundary conditions at $x=0$ and L can be expressed as

$$\begin{cases} 1+u^R = U_1 + U'_1, \\ \mu_1 ik_1 (1-u^R) = \mu_2 ik_2 (U_1 - U'_1), \\ U_1 e^{i\delta_1} + U'_1 e^{-i\delta_1} = u^T, \\ \mu_2 ik_2 (U_1 e^{i\delta_1} - U'_1 e^{-i\delta_1}) = \mu_1 ik_1 u^T. \end{cases} \tag{14}$$

Eq. (14) can be divided into two equations, i.e.,

$$\begin{Bmatrix} 1 \\ 1 \end{Bmatrix} + \begin{Bmatrix} 1 \\ -1 \end{Bmatrix} u^R = \begin{bmatrix} 1 & 1 \\ \frac{1}{n_{21}} & \frac{-1}{n_{21}} \end{bmatrix} \begin{Bmatrix} U_1 \\ U'_1 \end{Bmatrix}, \quad \begin{bmatrix} e^{i\delta_1} & e^{-i\delta_1} \\ e^{i\delta_1} & -e^{-i\delta_1} \end{bmatrix} \begin{Bmatrix} U_1 \\ U'_1 \end{Bmatrix} = \begin{Bmatrix} 1 \\ 1 \end{Bmatrix} u^T. \tag{15}$$

Therefore,

$$\begin{Bmatrix} 1 \\ 1 \end{Bmatrix} + \begin{Bmatrix} 1 \\ -1 \end{Bmatrix} u^R = \mathbf{S}_1 \begin{Bmatrix} 1 \\ 1 \end{Bmatrix} u^T, \quad (16)$$

With

$$\mathbf{S}_1 = \begin{bmatrix} 1 & 1 \\ \frac{1}{n_{21}} & \frac{-1}{n_{21}} \end{bmatrix} \begin{bmatrix} e^{i\delta_1} & e^{-i\delta_1} \\ \frac{e^{i\delta_1}}{n_{21}} & \frac{-e^{-i\delta_1}}{n_{21}} \end{bmatrix}^{-1} = \begin{bmatrix} \cos \delta_1 & -in_{21} \sin \delta_1 \\ -i \sin \delta_1 / n_{21} & \cos \delta_1 \end{bmatrix}. \quad (17)$$

Inspired by this, the reflected wave u^R and transmitted wave u^T satisfy

$$\begin{Bmatrix} 1 \\ 1 \end{Bmatrix} + \begin{Bmatrix} 1 \\ -1 \end{Bmatrix} u^R = \mathbf{S} \begin{Bmatrix} 1 \\ 1 \end{Bmatrix} u^T = \begin{bmatrix} S_{11} & S_{12} \\ S_{21} & S_{22} \end{bmatrix} \begin{Bmatrix} 1 \\ 1 \end{Bmatrix} u^T, \quad (18)$$

In which $\mathbf{S} = \mathbf{S}_1 \mathbf{S}_2 \cdots \mathbf{S}_N$, $\mathbf{S}_m = \begin{bmatrix} \cos \delta_m & -in_{m+1m} \sin \delta_m \\ -i \sin \delta_m / n_{m+1m} & \cos \delta_m \end{bmatrix}$ and $m = 1, 2, \dots$. $n_{m+1m} = \frac{\rho_m \mu_m}{\rho_{m+1} \mu_{m+1}}$ is the impedance when the SH0 wave in Layer m travels into Layer $m+1$. Then

$$u^R = \frac{2}{S_{11} + S_{12} + S_{21} + S_{22}}, \quad u^T = \frac{S_{11} + S_{12} - S_{21} - S_{22}}{S_{11} + S_{12} + S_{21} + S_{22}}. \quad (19)$$

Especially, when $N=1$, u^R and u^T calculated from Eq. (18) have the same expressions as Eqs. (7) and (9), which can prove the theoretical correctness.

As numerical cases, $N=2$ (silicon/epoxy) and $N=3$ (silicon/epoxy/silicon) are respectively adopted to investigate the total transmission for SHM, and $L_1=L_2=L_3=L=1$ cm. Based on Eq. (19), I^R and I^T can be calculated, and shown in Fig. 9. Meanwhile, for comparison, the results from FEM are also depicted in Fig. 9. The results based on the transfer matrix method are the same as that from FEM, which once again prove the correctness of the theoretical model in this paper. Additionally, the maximum of I^T is not unit when $N=2$. However, the transmitted energy of SH0 waves can achieve a high level, nearly 96% when $f=0.356c_1/2L=57.84$ kHz, such as Fig. 10(b). It is not perfect total transmission, but the transmitted wave completely meets the needs of SHM applications. When $N=3$, the frequency corresponding for total transmission is $f=0.362c_1/2L$, which is slightly different from the case of $N=2$. The displacement distribution is shown in Fig. 10(d). Comparing Figs. 9(a) and 9(b), the bandwidth has been reduced evidently, which dues to the additional wave interference with the increasing number of layers.

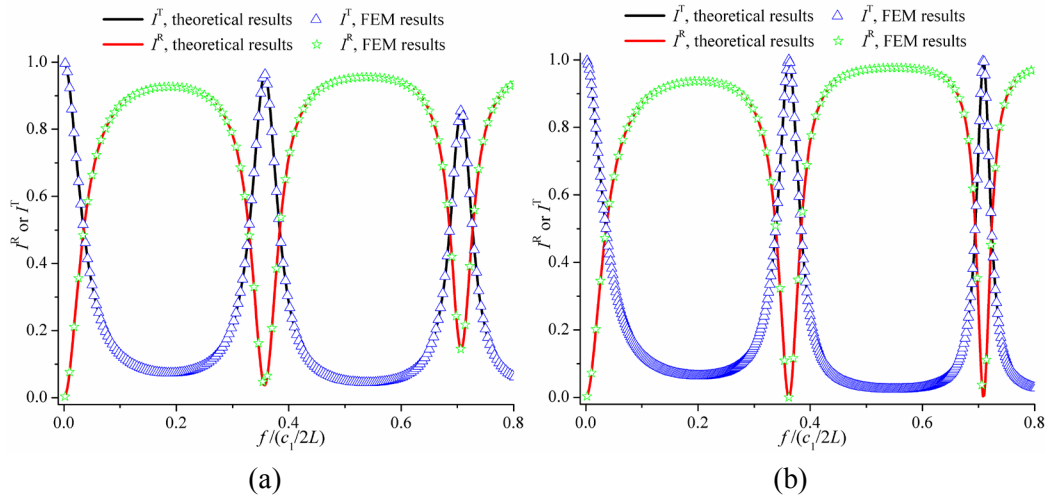


Figure 9: The theoretical and FEM results in Fig. 8: (a) $N=2$; (3) $N=3$

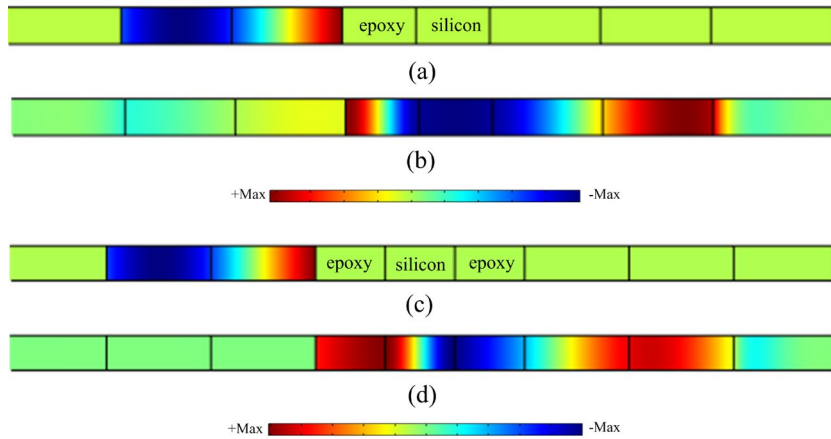


Figure 10: The displacement fields of SH0 waves: (a) is u_{in} ; (b) represents u^R and u^T when $N=2$, and $f=0.356c_1/2L=57.84$ kHz; (c) is u_{in} ; (b) represents u^R and u^T when $N=3$, and $f=0.362c_1/2L=58.48$ kHz

5 Conclusions

In summary, then frequency selection of SH0 waves for total transmission has been demonstrated in detail, in which three typical different structures are discussed. A systematical theoretical derivation is carried out, and the frequency corresponding for zero reflection is obtained and exemplified by FEM. It is revealed that an SH0 wave, with its wavelength equal to twice of the length of another medium in an inhomogeneous flat plate, can total transmit across this medium without reflection because of wave interference. Not limited by this, this phenomenon is suitable for a scraggy plate when the thickness variation is relatively small. To some extent, the methodology proposed here is general and adaptable in practice and our study also provides guidelines for guided wave manipulation in aeronautics and astronautics.

Acknowledgment: The authors gratefully acknowledge the supports by National Natural Science Foundation of China (Nos. 51408481, 51808439), Central University's special research funding special fund cross-disciplinary project (xj2017174), Natural Science Foundation Research Program of Shaanxi Province-Youth Talents Project (2013JQ7003).

Conflicts of Interest: The authors declare that they have no conflicts of interest to report regarding the present study.

References

- Belanger, P.; Boivin, G.** (2016): Development of a low frequency omnidirectional piezoelectric shear horizontal wave transducer. *Smart Materials and Structures*, vol. 25, no. 4, 045024.
- Cao, X. S.; Jin, F.; Jeon, I.; Lu, T. J.** (2009): Propagation of love waves in a functionally graded piezoelectric material (FGPM) layered composite system. *International Journal of Solids and Structures*, vol. 46, pp. 4123-4132.
- Dai, H.; Jing, X. J.; Sun, C.; Wang, Y.; Yue, X. K.** (2018): Accurate modeling and analysis of a bio-inspired isolation system: with application to on-orbit capture. *Mechanical Systems and Signal Processing*, vol. 109, pp. 111-133.
- Dai, H.; Jing, X. J.; Wang, Y.; Yue, X. K.; Yuan, J. P.** (2018): Post-capture vibration suppression of spacecraft via a bio-inspired isolation system. *Mechanical Systems and Signal Processing*, vol. 105, pp. 214-240.
- Danoyan, Z. N.; Piliposian, G. T.** (2008): Surface electro-elastic shear horizontal waves in a layered structure with a piezoelectric substrate and a hard dielectric layer. *International Journal of Solids and Structures*, vol. 45, pp. 431-441.
- Golub, M. V.; Fomenko, S. I.; Bui, T. Q.; Zhang, C. H.; Wang, Y. S.** (2012): Transmission and band gaps of elastic SH waves in functionally graded periodic laminates. *International Journal of Solids and Structures*, vol. 49, pp. 344-354.
- Kamal, A.; Giurgiutiu, V.** (2014): Shear horizontal wave excitation and reception with shear horizontal piezoelectric wafer active sensor (SH-PWAS). *Smart Materials and Structures*, vol. 23, no. 8, 085019.
- Lee, J. S.; Kim, Y. Y.; Cho, S. H.** (2009): Beam-focused shear-horizontal wave generation in a plate by a circular magnetostrictive patch transducer employing a planar solenoid array. *Smart Materials and Structures*, vol. 18, no. 1, 015009.
- Li, P.; Cheng, L.** (2017): Propagation of thickness shear waves in a periodically corrugated quartz crystal plate and its application exploration in acoustic wave filters. *Ultrasonics*, vol. 77, pp. 100-109.
- Li, P.; Cheng, L.** (2018): Shear horizontal wave propagation in a periodic stubbed plate and its application in rainbow trapping. *Ultrasonics*, vol. 84, pp. 244-253.
- Li, P.; Shan, S. B.; Wen, F. Z.; Cheng, L.** (2019): A fully-coupled dynamic model for the fundamental shear horizontal wave generation in a PZT activated SHM system. *Mechanical Systems and Signal Processing*, vol. 116, pp. 916-932.

- Lissenden, C.; Liu, Y.; Choi, G. W.; Yao, X.** (2014): Effect of localized microstructure evolution on higher harmonic generation of guided waves. *Journal of Nondestructive Evaluation*, vol. 33, pp. 178-186.
- Miao, H.; Dong, S.; Li, F.** (2016): Excitation of fundamental shear horizontal wave by using face-shear (d_{36}) piezoelectric ceramics. *Journal of Applied Physics*, vol. 119, no. 17.
- Mitra, M.; Gopalakrishnan, S.** (2016): Guided wave based structural health monitoring: a review. *Smart Materials and Structures*, vol. 25, no. 5, 053001.
- Pennec, Y.; Djafari-Rouhani, B.; Larabi, H.; Vasseur, J. O.; Hladky-Hennion, A. C.** (2008): Low-frequency gaps in a phononic crystal constituted of cylindrical dots deposited on a thin homogeneous plate. *Physical Review B*, vol. 78, no. 10, 104105.
- Pruell, C.; Kim, J. Y.; Qu, J. M.; Jacobs, L. J.** (2009): Evaluation of fatigue damage using nonlinear guided waves. *Smart Materials and Structures*, vol. 18, no. 3, 035003.
- Qian, Z. H.; Liu, N.; Yang, J. S.; Hirose, S.** (2010): Propagation of thickness-twist waves in a piezoelectric ceramic plate in contact with viscous fluids. *Acta Mechanica*, vol. 212, pp. 263-270.
- Sarvazyan, A. P.; Rudenko, O. V.; Swanson, S. D.; Fowlkes, J. B.; Emelianov, S. Y.** (1998): Shear wave elasticity imaging: a new ultrasonic technology of medical diagnostics, *Ultrasound in Medicine & Biology*, vol. 24, pp. 1419-1435.
- Stepinski, T.; Mańka, M.; Martowicz, A.** (2017): Interdigital Lamb wave transducers for applications in structural health monitoring. *Nondestructive Testing and Evaluation International*, vol. 86, pp. 199-210.
- Wang, Q.; Quek, S. T.; Varadan, V. K.** (2005): Analytical solution for shear horizontal wave propagation in piezoelectric coupled media by interdigital transducer. *American Society of Mechanical Engineers Journal of Applied Mechanics*, vol. 72, pp. 341-350.
- Wilcox, P. D.; Cawley, P.; Lowe, M. J. S.** (1998): Acoustic fields from PVDF interdigital transducers. *IEE Proceedings on Science, Measurement and Technology*, vol. 145, pp. 250-259.
- Xu, Y. L.** (2015): Spatial bandwidth enlargement and field enhancement of shear horizontal waves in finite graded piezoelectric layered media. *Physics Letters A*, vol. 379, pp. 1752-1756.
- Zhou, W. S.; Li, H.; Yuan, F. G.** (2015): Fundamental understanding of wave generation and reception using d_{36} type piezoelectric transducers. *Ultrasonics*, vol. 57, pp. 135-143.
- Zhu, J.; Chen, W. Q.; Yang, J. S.** (2014): Propagation of thickness-twist waves in elastic plates with periodically varying thickness and phononic crystals. *Ultrasonics*, vol. 54, pp. 1899-1903.